provided that PDP is linear or has a constant degree of branching. As the melt HCTP was difficult to clarify, we have not been able to determine R_{vu} for pure HCTP directly. However, we did succeed in determining R_{vu} for HCTP by two independent methods (to within 50%). Fortunately, at sufficiently high PDP concentration in HCTP, R_{vu} (solution) $\gg R_{vu}$(HCTP). Thus, we were able to estimate the excess Rayleigh ratio in the dilute solution regime. Time correlation function measurements are feasible. However, very precise measurements that could warrant correlation function profile analysis were not made because the melt could not be prepared as dust-free as the monomer in TCB solution. Some cooperative diffusion coefficient results are presented. Future results refer to the solution polymerization of HCTP (Paper 2) for a more detailed and fruitful analysis.

Acknowledgment. We gratefully acknowledge support of this work by the US Army Research Office and the Army Materials Technology Laboratory. G.F. thanks B.C. for his hospitality while working in his laboratory.

Registry No. I (SRU), 26085-02-9; II, 940-71-6; II (homopolymer), 25231-98-5.

References and Notes

(1) Allcock, H. R. *Chem. Eng. News* **1985**, *63*, 22.
(2) Singler, R. E.; Hagnauer, G. L.; Sicka, R. W. *ACS Sym. Ser.* **1984**, *260*, 143.
(3) Singler, R. E.; Hagnauer, G. L.; Sicka, R. W. *ACS Symp. Ser.* **1982**, *193*, 229.
(4) Hagnauer, G. L *J. Macromol. Sci. Chem.* **1981**, *A16* (1), 385.
(5) Sennett, M. S.; Hagnauer, G. L.; Singler, R. E.; Davies, G. *Macromolecules*, in press.
(6) Hagnauer, G. L.; Singler, R. E.; *Org. Coat. Plast. Chem.* **1979**, *44*, 88.
(7) Hagnauer, G. L. *ACS Symp. Ser.*, **1980**, *138*, 239.
(8) Hagnauer, G. L.; Koulouris, T. N. *Chromatogr. Sci.* **1981**, *19*, 99.
(9) de Gennes, P.-G. *Scaling Concepts in Polymer Physics*; Cornell University: Ithaca, NY, 1979; Chapter 1, pp 29-53.
(10) Huglin, M. B., Ed. *Light Scattering from Polymer Solutions*; Academic: New York, 1972.
(11) Kerker, M. *Scattering of Light and Other Electromagnetic Radiation*; Academic: New York, 1969.
(12) Chu, B.; Fytas, G.; Zalczer, G. *Macromolecules* **1981**, *14*, 395.
(13) Sears, W. M.; Hunt, J. L.; Stevens, J. R. *J. Chem. Phys.* **1981**, *75*, 1589.
(14) Sears, W. M.; Hunt, J. L.; Stevens, J. R. *J. Chem. Phys.* **1981**, *75*, 1599.
(15) Gulari, E.; Mckeigue, K.; Ng, K. Y. S. *Macromolecules* **1984**, *17*, 1822.
(16) Loy, B. R.; Chrisman, R. W.; Nyquist, R. A.; Putzig, C. L. *Appl. Spectrosc.* **1979**, *23*, 174.
(17) Chu, G. *Laser Light Scattering*; Academic: New York, 1974. Berne, B. J.; Pecora, R. *Dynamic Light Scattering*; Wiley: New York, 1976.
(18) Chu, B. In *Scattering Techniques Applied to Supramolecular and Nonequilibrium Systems*; Chen, S.-H., Chu, B., Nossal, R., Eds.; Plenum: New York, 1981, pp 231-264.
(19) Allcock, H. R.; Arcus, R. A. *Macromolecules* **1979**, *12*, 1130.
(20) Simha, R.; Boyer, R. F. *J. Chem. Phys.* **1962**, *37*, 1003.
(21) Boyer, R. F.; Spencer, R. S. *J. Appl. Phys.* **1944**, *15*, 398.
(22) Painter, P. C.; Zarian, J.; Coleman, M. M. *Appl. Spectrosc.* **1982**, *36*, 265.
(23) Zarian, J.; Painter, P. C.; Coleman, M. M. *Appl. Spectrosc.* **1982**, *36*, 272.
(24) Coleman, M. M.; Zarian, J.; Painter, P. C. *Appl. Spectrosc.* **1982**, *36*, 277.
(25) Huglin, M. B.; Sokro, M. B. *Polymer* **1980**, *18*, 651.
(26) Ohta, T.; Oono, Y. *Phys. Lett.* **1982**, *89A*, 460.
(27) Chu, B.; Lee, D.-Ç. *Macromolecules* **1984**, *17*, 926.
(28) Wiltzius, P.; Haller, H. R.; Cannell, S. D. *Phys. Rev. Lett.* **1983**, *51*, 1183.

Application of Raman and Laser Light Scattering to the Solution Polymerization of Hexachlorocyclotriphosphazene. 2.

Benjamin Chu* and Day-chyuan Lee†

Department of Chemistry, State University of New York at Stony Brook, Long Island, New York 11794-3400. *Received November 4, 1985*

ABSTRACT: Poly(dichlorophosphazene) (PDP) can be synthesized by either thermal polymerization of melt hexachlorocyclotriphosphazene (HCTP), as discussed in paper 1, or solution polymerization of HCTP in various solvents. In solution polymerization in the presence of a mixed solvent containing varying amounts of trichlorobenzene (TCB) and HCTP, we have taken into account the effects due to preferential adsorption by refractive index matching of cosolvents that happen to become isorefractive at 110 °C. We have succeeded in determining the molecular parameters, including concentrations of the monomer (C_m) and the polymer (C_p), as well as properties of the polymer product (PDP), such as the weight-average molecular weight (M_w), the second virial coefficients (A_2 and d_d), the z-average radius of gyration (R_g), and the hydrodynamic radius (R_h) in the dilute solution regime, and the cooperative diffusion coefficient (D_c) as well as the osmotic compressibility $[(\partial\pi/\partial C)_{T,P}]$ in semidilute solutions. With precise intensity-intensity time correlation function measurements, we have also succeeded in estimating the polymer molecular weight distribution of PDP during the polymerization process. The development of the present methodology in characterizing PDP in situ avoids the decomposition of PDP by moisture and has the potential to become a practical approach to investigate the solution polymerization of HCTP under a variety of conditions, including judicial use of catalysts. Its eventual development for monitoring specific polymerization processes in situ has become a possibility worthy of consideration.

Introduction

In paper 1, we have shown how thermal polymerization of melt hexachlorocyclotriphosphazene (HCTP) can be monitored in situ by using a combination of laser Raman and light scattering. In our data analysis, we took advantage of Raman spectroscopy to determine the concentration of the polymer (poly(dichlorophosphazene), PDP) in HCTP and a combination of static light scattering intensity and dynamic Rayleigh line width measurements to characterize some of the macromolecular properties of PDP, an important precursor to so many organophosphazene polymers. In this paper (2), we extend our

† Present address: Chemical Engineering Department, University of Wisconsin, Madison, Wisconsin 57305.

0024-9297/86/2219-1592$01.50/0

application to the solution polymerization of HCTP. The presence of an additional solvent [in our case, 1,2,4-trichlorobenzene (TCB)] permits the polymerization process to be carried out at a somewhat lower temperature (215 °C instead of 250 °C), yields PDP of narrower molecular weight distributions, and has a more controllable polymerization reaction. In addition, we can introduce catalysts and try to optimize conditions for the polymerization process. Thus, our development of an in situ method to determine polymer concentration and to characterize macromolecular properties of the polymer product in the presence of a mixed solvent is a very useful step toward eventual improvements in quality and our understanding of organophosphazene polymers.

Preferential adsorption becomes an important complication in the characterization of polymers in a mixed solvent. In this article, we offer a specific solution to the problem, i.e., by means of refractive index matching, a difficult light scattering problem resolved by a unique optical solution. As the procedures are, otherwise, the same as in paper 1, we shall describe only those steps that differ from the thermal polymerization of HCTP, provide the physical properties that are essential in our analysis, and discuss the results in detail.

Theoretical Background

Intensity of Scattered Light.[1] The excess Rayleigh ratio, R_{vu} (cm^{-1}), at finite concentrations in dilute solution has the approximate form

$$HC/R_{vu} = (1/M_w)(1 + K^2R_g^2/3) + 2A_2C \quad (1)$$

where H (in units of mol cm^2 g^{-2}) is equal to $4\pi^2n^2(dn/dC)^2/(N_A\lambda_0^4)$ with n, C (g/cm^3), N_A, λ_0, and dn/dC being respectively the refractive index, the concentration, Avogadro's number, the wavelength of light in vacuo, and the refractive index increment. Subscripts vu denote vertically polarized incident and unpolarized scattered light, A_2 (mol cm^3 g^{-2}) is the second virial coefficient, K [$=(4\pi/\lambda)\sin(\theta/2)$] is the magnitude of the momentum transfer vector with λ [$=\lambda_0/n$] and θ being the wavelength of light in the scattering medium and the scattering angle, respectively.

Equation 1 is valid for a polymer solution consisting of a single solvent. For a polymer chain dissolved in a mixed solvent, the interpretation of light scattering data becomes more complex. Since the two solvents have different affinities for the same polymer chain, one of the solvents reacts preferentially with the polymer, and a difference in the solvent composition near the polymer molecule with respect to the overall solvent composition will occur. By considering the polymer chain plus the excess amount of the solvent as a new polymer complex, eq 1 can be used to describe the behavior of the polymer complex in the mixed solvent. The refractive index increment for the new polymer complex $(dn/dC)_t$ can be defined as[1]

$$(dn/dC)_t = (dn/dC)_v + A_p(n_m - n_t) \quad (2)$$

where $(dn/dC)_v$ is the refractive index increment of the polymer solution at constant solvent composition, A_p is the preferential adsorption coefficient, and n_m and n_t are the refractive indexes of solvent m (HCTP) and t (TCB), respectively.

By the definition of the refractive index increment for the polymer complex, eq 1 can be modified as follows for a mixed solvent:

$$\frac{H^\dagger C}{R_{vu}} = \left(\frac{1}{M_w}\right)\left(1 + \frac{16\pi^2n^2}{3\lambda_0^2}R_g^2\sin^2\left(\frac{\theta}{2}\right)\right) + 2A_2C \quad (3)$$

where $H^\dagger$, in units of mol cm^2 g^{-2}, is equal to $4\pi^2n^2(dn/dC)_t^2/(N_A\lambda_0^4)$ with $(dn/dC)_t$ defined by eq 2. If we were to treat the polymer in a mixed solvent in a way analogous to a single solvent, the apparent properties can be described as

$$\frac{H^*C}{R_{vu}} = \left(\frac{1}{M_{w,app}}\right)\left(1 + \frac{16\pi^2n^2}{3\lambda_0^2}R_g^2\sin^2\left(\frac{\theta}{2}\right)\right) + 2A_{2,app}C \quad (4)$$

where H^*, in units of mol cm^2 g^{-2}, is equal to $4\pi^2n^2(dn/dC)_v^2/(N_A\lambda_0^4)$ with $(dn/dC)_v$ replacing $(dn/dC)_t$ in $H^\dagger$ of eq 2, $M_{w,app}$ is the apparent molecular weight, and $A_{2,app}$ is the apparent second virial coefficient.

Diffusion Coefficients. At finite concentrations the translational diffusion coefficient can be expressed as

$$D = (C/f)(\partial\mu/\partial C) \quad (5)$$

where f is a friction coefficient. Thus, we can see that the diffusion coefficient is composed of two factors, a "hydrodynamics" factor, $1/f$, and a "thermodynamics" factor $(\partial\mu/\partial C)$. The thermodynamics force serves as the driving force and the hydrodynamics force as a dragging force.

The $(\partial\mu/\partial C)$ term can be related to the osmotic compressibility by the relation

$$\left(\frac{\partial\mu}{\partial C}\right) = \left(\frac{M(1 - \bar{v}_2C)}{C}\right)\left(\frac{\partial\pi}{\partial C}\right) \quad (6)$$

where $\bar{v}_2$ is the partial specific volume of the polymer.

At infinite dilution only frictional properties are important

$$D_0 = k_BT/f_0 \quad (7)$$

where the subscript 0 indicates infinite dilution and k_B is the Boltzmann constant. The friction coefficient can be related to the hydrodynamic radius R_h through the Stokes–Einstein relation

$$f_0 = 6\pi\eta R_h \quad (8)$$

where η is the solvent viscosity.

The diffusion coefficient at infinite dilution can be expressed by a scaling relation

$$D_0 = k_DM_w^{-\alpha_D} \quad (9)$$

where k_D and α_D are constants and can be determined experimentally.

At finite concentrations in the dilute solution regime

$$D = D_0(1 + k_dC) \quad (10)$$

where k_d is the second virial coefficient for diffusion and is system specific.

Correlation Function Profile Analysis.[2-6] Given the fact that translational diffusion for one molecular weight will produce a single-exponential decay with a characteristic line width Γ for the scattered electric field time correlation function $g^{(1)}(\tau)$, adding additional molecules of different molecular weights into the scattering volume will result in a distribution of exponentials as

$$g^{(1)}(\tau) = \sum_i W_i \exp(-\Gamma_i\tau) \quad (11)$$

where W_i ($\propto I_i$) is the normalized intensity weighting factor of each representative molecular weight fraction M_i. It should be noted that I_i also changes with K for large particles ($KR_{g,i} \gtrsim 1$) even for the (vv) polarized component of the Rayleigh ratio.

In the continuous limit, eq 11 becomes

$$g^{(1)}(\tau) = \int_0^\infty G(\Gamma) \exp(-\Gamma\tau)\, d\Gamma \quad (12)$$

where $G(\Gamma)$ is the normalized distribution of characteristic line widths. In practice, eq 12 uses a measured $g^{(1)}(\tau)$ that has noise and is bandwidth limited. Furthermore, the limits of integration have both upper (b) and lower (a) bounds, yielding

$$g^{(1)}(\tau) = \int_a^b G(\Gamma) \exp(-\Gamma\tau)\, d\Gamma \quad (13)$$

As the Laplace inversion of eq 13 is ill-conditioned, we can only approximate $G(\Gamma)$ and restrict our discussion to the solution of eq 13 according to the method of regularization.[6]

In the presence of additive noise $R(\tau)$ and with bandwidth-limited signals, we rewrite eq 13 such that[6]

$$B(\tau) = \int_{\Gamma_{min}}^{\Gamma_{max}} O(\tau,\Gamma)G(\Gamma)\, d\Gamma + R(\tau) \quad (14)$$

In operator form

$$B = OG + R \quad (15)$$

A regularized approximation to the true distribution function was obtained by minimizing the functional

$$F(U) = \|B - OU\|^2 + \alpha_s\|LU\|^2 \quad (16)$$

where U represents the possible set of functions satisfying eq 16, α_s is the regularization parameter, and L is any linear constraint operator that allows the incorporation of additional a priori knowledge of the solution. α_s should be chosen as small as possible to avoid oversmoothing.

Once we have the continuous distribution in Γ space, we can then transform it to the molecular weight space. With the combination of eq 4 and 12 and in the limit of short delay time

$$\langle I(K)\rangle = \langle E^*(K,0)E(K,0)\rangle = \lim_{\tau\to 0} g^{(1)}(K,\tau) = \lim_{\tau\to 0} \int_a^b G(K,\Gamma)e^{-\Gamma\tau}\, d\Gamma \quad (17)$$

According to eq 1, 9, 17, and $I(K) = Ni(K)$, we can relate each fraction (j) by

$$f_w(M_j) \sim \frac{G_j(\Gamma_j)[1 + K^2R_{gj}^2(M_j)/3 + 2\bar{A}_2CM_j]}{M_j^{\alpha_D+2}} \quad (18)$$

where $f_w(M_j)$ is the weight fraction of representative polymer molecules with molecular weight M_j and $G_j(\Gamma_j)$ is the corresponding scattered intensity from M_j polymer molecules. In eq 18, we have taken $P^{-1} \sim 1 + K^2R_g^2/3$ and $\bar{A}_2$ to be the measured second virial coefficient over an effective molecular weight distribution range. In the limit of zero angle and zero concentration the particle scattering factor $P(KR_g) = 1$ and eq 18 can be simplified to

$$f_w(M_j) \sim \frac{G_j(\Gamma_j)}{M_j^{\alpha_D+2}} \quad (19)$$

Experimentally, we used eq 13 to estimate a continuous line width distribution. We then used a fixed number of representative fractions to do the transformation. In a discrete representative distribution of $G_j(\Gamma_j)$ vs. Γ_j, the transform of Γ_j to molecular weight M_j along the x axis was accomplished by the relation $\Gamma = DK^2$ and eq 9. The transformation along the y axis was accomplished by eq 18.

In our iterative procedure, we first estimated k_D by assuming that $P(kR_g) = 1$ and then adjusted k_R by comparing the measured and computed R_g values using the first approximate $f_w(M_j)$. We varied k_D by comparing the measured and the computed values of M_w. The iterative procedure continued until we arrived at a k_D value that yielded a $M_{w,calcd}$ in agreement with the measured M_w from our static light scattering measurements. For completeness we note that

$$M_{w,calcd} = \frac{\int f_w M\, dM}{\int f_w\, dM} \quad (20)$$

$$R_{g,calcd} = k_R \frac{\int f_w M^{1+\alpha_R}\, dM}{\int f_w M\, dM} \quad (21)$$

and

$$F_{w,cum} = \frac{\int_M^\infty f_w(M)\, dM}{\int_0^\infty f_w(M)\, dM} \quad (22)$$

where $F_{w,cum}(M)$ is the normalized cumulative weight-average molecular weight distribution.

Experimental Methods

Light Scattering Spectrometer. The light scattering spectrometer used for this study measures the angular distribution of absolute scattered intensity, the intensity–intensity time correlation function, and the Raman intensity and has been described in Part 1.

Sample Preparation. HCTP was prepared by Dr. Gary Hagnauer of MTL at Watertown, MA. HCTP was purified by recrystallization from heptane and vacuum sublimed to remove all traces of water and tetramer.

1,2,4-Trichlorobenzene (Fisher Scientific Co., HPLC grade) (TCB) was dried over anhydrous $CaCl_2$ for 3 days and fractionally distilled under vacuum. The solutions used for solution polymerization were prepared as follows. Trimer (HCTP) (29%–30%) in 1,2,4-trichlorobenzene was heated to 45 °C and then filtered through a Millipore filter of nominal 0.5-μm pore diameter. All samples were degassed by several freeze–pump cycles and flame sealed under vacuum.

Physical Constants. We used benzene as a reference with $R_{vu} = R_{vv} + R_{vh} = 3.86 \times 10^{-5}$ cm^{-1} for benzene at $\theta = 90°$, $\lambda_0 =$ 488 nm and 23 °C.

TCB. Both refractive index and density data were adapted from ref 9 and fitted with least-squares procedures to get analytical expressions for the temperature dependence of refractive index and of density; d_t (g/cm^3) $= 1.48 - 1.28 \times 10^{-3}t_c$, with t_c expressed in degrees Celsius, and $n_t = 1.59 - 4.46 \times 10^{-4}t_c$ at wavelength 488 nm were obtained. For the temperature dependence of the refractive index, the original data were measured at the sodium D line and corrected to the proper wavelength by assuming that TCB had the same dispersion factor as benzene.

PDP. The refractive index increment was measured at three different temperatures, 30, 140, and 170 °C. At 250 °C and for PDP/HCTP, we determined $(dn/dC)_v$ $[=(dn/dC)_t] = (n_c - n_m)/C$ with n_c and n_m measured with the same lens refraction technique and the subscripts c and m denoting solution and HCTP, respectively. The refractive index of PDP could then be calculated by using the L–L2 equation (see Chapter V, eq 55 of ref 1) and the dn/dC result.

Mixed Solvent HCTP/TCB. Viscosity of the mixed solvent was measured by a Cannon–Fenske capillary viscometer from 40 to 95 °C. The expression ln η (cP) $= -2.51 + 9.59 \times 10^2(1/T)$ (K^{-1}) was obtained.

Results and Discussion

In calculating the refractive index increment of PDP in various solvents, the density is needed only in intermediate steps. From the measured refractive index increment in different solvents and at different temperatures, the tem-

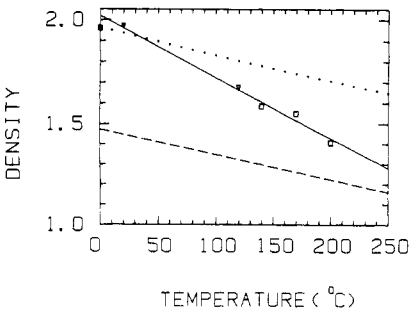

Figure 1. Plot of d_t, d_m, and d_p vs. temperature for monomer (open squares, this measurement; open inverted triangle, data from ref 7; filled inverted triangle, data from ref 8; solid line, fitting of hollow squares, d_m (g/cm^3) = 2.05 − 3.01 × 10$^{-3}t_c$ (°C)); for TCB solvent[9] (dashed line, d_t (g/cm^3) = 1.48 − 1.28 × 10$^{-3}t_c$ (°C)); for polymer (filled squares, data from ref 10; dotted line represents points estimated by an empirical equation $\alpha_1 T_g = 0.16$ or $\alpha_1 = 0.16/T_g \sim 7.12 \times 10^{-4}$ K^{-1}, with T_g being the glass transition temperature, d_p (g/cm^3) = 1.98 exp(−7.12 × 10$^{-4}t_c$ (°C)).

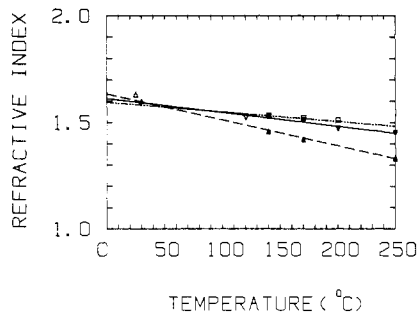

Figure 2. Plot of n_t, n_m, and n_p vs. temperature for monomer (inverted filled triangles, this measurement; inverted open triangles, ref 7; solid line, n_m = 1.62 − 6.71 × 10$^{-4}t_c$ (°C)); for TCB solvent (open squares, this measurement; dash–dot line, fitting from ref 9, n_t = 1.59 − 4.46 × 10$^{-4}t_c$ (°C)); for polymer (filled triangles, this measurement, open triangle, from ref 11; dashed line, n_p = 1.62 − 1.14 × 10$^{-4}t_c$ (°C)). The refractive index of the polymer is calculated from the dn/dC measurement using the Lorenz–Lorentz (L–L2) equation.[1] Subscripts t, m, and p denote TCB, HCTP, and PDP, respectively.

perature dependence of the polymer refractive index can be extracted from the same equation used to calculate the polymer refractive index increment. Therefore, the errors introduced in estimating the polymer density are not crucial. As shown in Figure 1 the temperature dependence of the density for PDP, similar to that of TCB, is roughly around −1 × 10^{-3} g cm^{-3} °C^{-1}, in reasonable agreement with that of other polymers listed in the *Polymer Handbook*. All physical measurements (density, refractive index, etc.) were checked with literature values as indicated in Figures 1 and 2, respectively. The viscosity of PDP in HCTP/TCB at different temperatures is shown in Figure 3.

Fractional Conversion of Monomer f_m (=1 − f_p). Several representative Raman spectra obtained during the course of solution polymerization of HCTP in TCB at 215 °C are shown in Figure 4. The concentration of polymer formed by solution polymerization, C_p (g/cm^3), is computed slightly differently from that of thermal polymerization and has the form

$$C_p = \frac{f_p d_t d_p d_m x_m^0}{d_p(d_m x_t^0 + f_m d_t x_m^0) + f_p d_t d_m x_m^0} \quad (23)$$

where d_m, d_p, and d_t are densities of HCTP, of PDP, and of TCB, in g/cm^3, respectively, and x_m^0 and x_t^0 are the initial weight fractions of HCTP and TCB, respectively. In eq 23, we have assumed no interaction between HCTP, PDP, and TCB, i.e., the volume of mixing is zero. We can

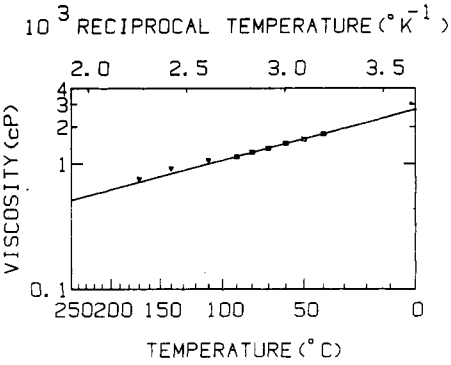

Figure 3. Plot of viscosity of mixed solvent (HCTP, 29% weight fraction, in TCB) vs. temperature: open squares represent data measured by Cannon–Fenske capillary viscometer, solid line represents fitted data, ln η (cP) = −2.51 + 9.59 × 10^2(1/T) (K^{-1}); open inverted triangles represent data from back calculation [by eq 7 and 8] of the correlation function taken at different temperatures for sample S4 at concentration C = 1.96 × 10^{-2} g/cm^3 and 30° scattering angle (Figure 17).

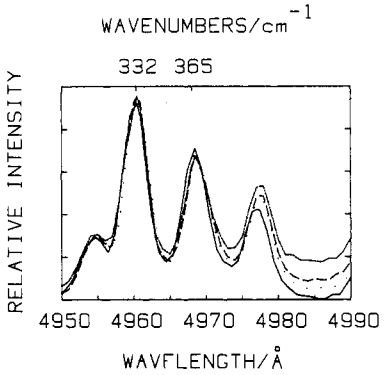

Figure 4. Several Raman spectra obtained during the course of solution polymerization of hexachlorocyclotriphosphazene at 215 °C showing the decrease in P–Cl$_2$ symmetric stretching peak at 365 cm^{-1} and the constant intensity at 332 cm^{-1} contributed from TCB for sample S2 at 1 h (solid line), 113 h (dotted line), 285 h (dashed line), and 430 h (dash–dot line).

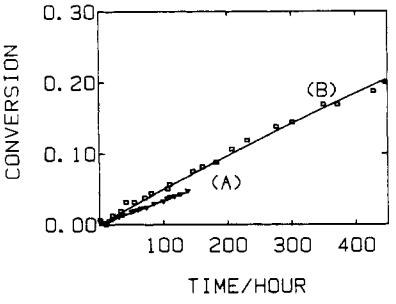

Figure 5. Fractional conversion of monomer vs. time obtained from the height change of the PCl$_2$ peak for sample S1 (inverted open triangles, experimental data; solid line A, fitted curve) and S2 (hollow squares, experimental data; solid line B, fitted curve) at 215 °C. The solid lines A and B for samples S1 and S2 were fitted according to $f_p = 1 - \exp(-a_1 t)$ with a_1 values listed in Table I.

also see that the second term in the denominator can be neglected as long as $d_p(d_m x_t^0 + f_m d_t x_m^0) \gg f_p d_t d_m x_m^0$. In this experiment, $f_p < 0.3$, implying that 17 ≫ 1. So an error in the estimation of density of the PDP polymer is not important in calculating the polymer concentration. The fractional conversion of monomer as a function of time in solution polymerization can still be represented by $f_p = 1 - \exp(-a_1 t)$, with the numerical values for a_1 listed in Table I. Figure 5 shows plots of fractional conversion of monomer vs. time for samples S1 and S2. It should be noted that the reaction rate of solution polymerization is

Table I
Fitting Parameters in Evaluating the Time Dependence of the Fractional Conversion of Monomer during the Solution Polymerization of Hexachlorocyclotriphosphazene in TCB at 215 °C[a]

sample (init wt % HCTP)	a_1, h^{-1}
S1 (29)	3.43×10^{-4}
S2 (29)	5.10×10^{-4}
S3 (29)	1.00×10^{-3}
S4 (29)	1.20×10^{-3}
S5 (25)	1.30×10^{-3}

[a] $f_p = 1 - \exp(-a_1 t)$.

very sensitive to even a trace amount of moisture or impurity in HCTP.

Intensity of Scattered Light. By means of Raman scattering, we can determine the polymer concentration C_p at any time during the polymerization process. We shall now combine this information with light scattering (intensity) measurements to examine the molecular properties of the polymer product formed. As illustrated in ref 12 and 13, such a combination should provide us with useful information about the molecular properties of the polymer formed without disturbing the polymerization reaction, thus eliminating any possibility of cross-linking the PDP induced by contact with trace amounts of additional moisture during transfer of PDP for analysis. Since HCTP is a solid at room temperatures and the melting point of HCTP is around 110 °C, it is difficult to prepare a dust-free HCTP melt for light scattering studies. In a solution polymerization the analysis of the intensity of the scattered light is complicated by the preferential adsorption effect. The two solvents (HCTP and TCB) have different affinities for the polymer (PDP). This will result in a difference of solvent composition near the polymer molecule with respect to the overall solvent composition. Equations 2–4 should be used to take the preferential adsorption effect into account. Furthermore, in the solution polymerization process one of the solvents (HCTP) is involved in the polymerization reaction. Thus the amount of HCTP is a decreasing function with respect to reaction time, and the composition of the mixed solvent (HCTP/TCB) changes with reaction time. The change in solvent composition changes the refractive index of the mixed solvent as well as the refractive index increment of the polymer in the mixed solvent. In order to follow the change of refractive index with respect to reaction time we used the Lorenz–Lorentz formula 1 (L–L1), which is well established for binary solvent mixtures[1]

$$\frac{n_s^2 - 1}{n_s^2 + 2} = d_s\left[\frac{x_t}{d_t}\left(\frac{n_t^2 - 1}{n_t^2 + 2}\right) + \frac{x_m}{d_m}\left(\frac{n_m^2 - 1}{n_m^2 + 2}\right)\right] \quad (24)$$

where d_s is the density of the mixed solvent, $d_x = d_m d_t/(x_t d_m + x_m d_t)$ with x_m [$=f_m x_m^0/(f_m x_m^0 + x_t^0)$], and x_t [$=1 - x_m$] being the weight fraction of HCTP and TCB in the mixed solvent during the reaction.

To calculate the refractive index increment of the polymer in a mixed solvent, we used the L–L formula 2 (L–L2)[1]

$$\left(\frac{dn}{dC}\right)_v = \frac{1}{d_p}\left(\frac{n_p^2 - 1}{n_p^2 + 2} - \frac{n_s^2 - 1}{n_s^2 + 2}\right)\frac{(n_s^2 + 2)^2}{6n_s} \quad (25)$$

where $(dn/dC)_v$ is the refractive index increment of the solution *at constant solvent composition*. The L–L2 formula is well established for polymer–single solvent systems. The applicability of L–L2 formula to mixed solvents was checked by comparing the calculations with literature values for PMMA/TFP/water[14] and PMMA/MMA/acetonitrile[15] systems. The deviation between calculated and literature values is within 2%, as shown in Table II. Similar comparisons were available in the literature[16,17] in which the Gladstone and Dale[18] formula was used. To determine the weight-average molecular weight of polymer in solution by light-scattering intensity measurements, we needed to know the absolute scattered intensity at the measuring temperature t_c (=215 °C) and the incident wavelength λ_0 (=488 nm). The excess Rayleigh ratio of a polymer in a mixed solvent at a given temperature can be computed by the relation

Table II
Comparison of Estimated $(dn/dC)_v$ Values by L–L2 Formula (eq 25) with Measured Values

vol fract solvent[a]	measd	calcd	dev, %
PMMA/MMA/acetonitrile			
0.17	0.091	0.092	2.1
0.32	0.100	0.101	1.0
0.50	0.110	0.110	0.0
0.68	0.119	0.120	0.8
PMMA/2,2,3,3-tetrafluoropropanol/water			
0.95	0.141	0.139	1.4
0.90	0.139	0.138	0.7
0.80	0.135	0.137	1.4
0.70	0.133	0.135	1.5
0.65	0.132	0.134	1.5

[a] Acetonitrile in PMMA/MMA/acetonitrile system and TFP in PMMA/2,2,3,3-tetrafluoropropanol/water system.

$$R_{vu}{}^t = \frac{(I^t_{vu,c}\exp(A_b C) - I^t_{vu,s})}{I^{25}_{B,vu}} R^{25}{}_{vu}\frac{n_s{}^t}{n_B{}^{25}} \quad (26)$$

where the subscript vu and the superscript t denote vertically polarized incident and unpolarized scattered beams and temperature, respectively. The term $n_s{}^t/n_B{}^{25}$ corrects for the scattering volume change due to refraction and is valid for our light scattering spectrometer based on the slit–pinhole detector geometry. The term $I^t_{vu,c}$ is the intensity of the polymer solution at elevated temperature t. The term $\exp(A_b C)$ corrects the effect of absorption, where C is the concentration and A_b is the absorption coefficient determined experimentally. The $I^t_{vu,s}$ term denotes the intensity of the mixed solvent at elevated temperature t. Strictly speaking this term is a variable with respect to the composition change of the mixed solvent. However, the change of the mixed-solvent intensity in the range of our measurement (25% HCTP in TCB to 29% HCTP in TCB) is less than 4%. Thus, it can be treated as a constant over the entire reaction period. This effect is being mentioned in the event that large variations of the solvent composition are encountered. The intensity of scattered light at four different scattering angles (30°, 60°, 90°, and 135°) was measured. By combining the concentration measured during the reaction with intensity measurements, we can calculate the quantity $H^*C/R_{vu}(\theta)$ at each moment. By extrapolation to zero scattering angle and subtraction of scattered intensity of HCTP/TCB, we have determined the excess Rayleigh ratio at zero scattering angle $R_{vu}(\theta=0)$ as a function of concentration.

For the living polymerization or condensation polymerization processes the molecular weight of the polymer produced will increase with respect to the conversion. On the other hand for addition polymerization processes the molecular weight of the polymer produced remains relatively constant during the initial polymerization process. The mechanism of the polymerization of HCTP is not completely known, but there is a great deal of evidence favoring the cation type polymerization. We first assumed

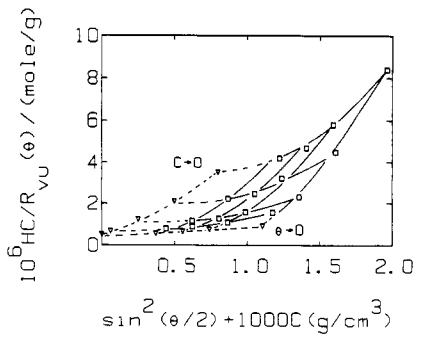

Figure 6. Zimm plot for sample S3, 29% HCTP in TCB polymerized at 215 °C and measured at 215 °C. From this Zimm plot $M_{w,app} \simeq (2.0 \pm 0.1) \times 10^6$, $A_{2,app} \simeq (4.0 \pm 0.2) \times 10^{-4}$ mol cm^3 g^{-2}, and $R_g \simeq 95 \pm 6$ nm were obtained. Note: H denotes H^* for Figures 6–9.

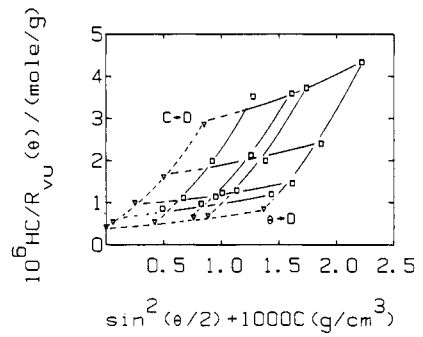

Figure 7. Zimm plot for sample S3 29% HCTP in TCB polymerized at 215 °C but measured at 110 °C. From this Zimm plot $M_w \simeq (2.5 \pm 0.1) \times 10^6$, $A_2 \simeq (3.1 \pm 0.2) \times 10^{-4}$ mol cm^3 g^{-2}, and $R_g \simeq 94 \pm 6$ nm were obtained.

that the molecular weight of the PDP product did not change in the dilute solution regime and then tried to verify this assumption later on. If the molecular weight remains constant, the Zimm plot can reveal most of the static molecular properties in the dilute solution regime. A typical Zimm plot is illustrated in Figure 6 for sample S3. In a mixed-solvent system such a Zimm plot can give us information about the apparent molecular weight, $M_{w,app}$, the apparent second virial coefficient, $A_{2,app}$, and the radius of gyration, R_g, of the polymer product formed according to eq 4. The polymer concentration C_p was determined by means of eq 23 using conversion data of Figure 5 obtained from Raman scattering. The apparent molecular weight has no physical meaning in itself but can be related to the true molecular weight through[1]

$$M_{w,app} = M_w\left(1 + A_p\frac{(n_m - n_t)}{(dn/dC)_v}\right)^2 \qquad (27)$$

If we do not know the preferential adsorption factor at the elevated temperature we cannot determine the true molecular weight in a mixed solvent. However, this difficulty can be overcome because there is a particular temperature and wavelength that will make the refractive index of HCTP and that of TCB equal. The light scattering measurements in an isorefractive solvent mixture are no longer affected by any possible preferential adsorption. The refractive index of HCTP and that of TCB match at 110 °C, as shown in Figure 2. Thus we can measure the scattered intensity of the reaction mixture at the same concentration as that at 215 °C by simply lowering the reaction temperature to 110 °C. The question whether the polymerization reaction becomes measurable at 110 °C can be checked by comparing the intensity of scattered light at 215 °C before and after the measurement

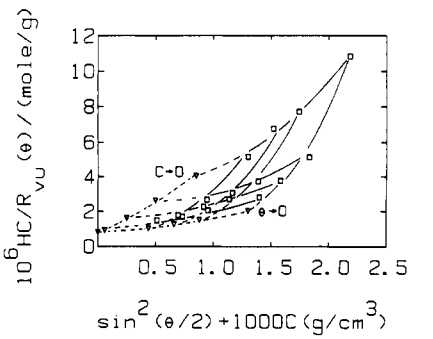

Figure 8. Zimm plot for sample S4 29% HCTP in TCB polymerized at 215 °C and measured at 215 °C. From this Zimm plot, $M_{w,app} \simeq (1.25 \pm 0.06) \times 10^6$, $A_{2,app} \simeq (4.5 \pm 0.3) \times 10^{-4}$ mol cm^3 g^{-2}, and $R_g \simeq 80 \pm 5$ nm were obtained.

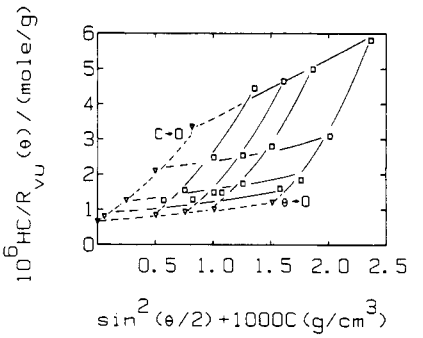

Figure 9. Zimm plot for sample S4 29% HCTP in TCB polymerized at 215 °C and measured at 110 °C. From this Zimm plot $M_w \simeq (1.56 \pm 0.08) \times 10^6$, $A_2 \simeq (3.6 \pm 0.2) \times 10^{-4}$ mol cm^3 g^{-2}, and $R_g \simeq 79 \pm 5$ nm were obtained.

at 110 °C. We observed no change in scattered intensity after restoring the temperature to 215 °C and concluded that there is negligible concentration change during our measurements at lower temperatures. Figure 7 illustrates a typical Zimm plot measured at 110 °C for the same sample S3. This procedure allows us to determine the true molecular properties without substantially disturbing the polymerization reaction. Once we have $M_{w,app}$ and M_w from the Zimm plots at 215 and 110 °C, we can calculate the effect due to preferential adsorption at 215 °C by means of eq 27 and recover the true second virial coefficient A_2 at 215 °C by using the relation

$$M_{w,app}A_{2,app} = M_wA_2 \qquad (28)$$

The same procedure was repeated for sample S4 as illustrated in Figures 8 and 9 measured at 215 and 110 °C, respectively. We found preferential adsorption to be relatively insensitive to molecular weight in our PDP/HCTP/TCB system. In run S4 we also measured the intensity of the scattered light at two other temperatures (140 and 170 °C) and found the preferential adsorption to be independent of temperature over the temperature range of our measurements, i.e., 110–215 °C. Furthermore the radius of gyration and the second viral coefficient also showed little temperature dependence. In run S5 we changed the starting composition of our binary mixture and repeated our studies. We found the preferential adsorption to be relatively independent of the composition of our solvent mixture, at least in the range 25 wt. % HCTP in TCB to 29 wt. % HCTP in TCB. The results are summarized in Table III. The radii of gyration listed in Table III were estimated through the quantity X_r, where $X_r = (KR_g)^2$. When $X_r \ll 1$ only the center of molecular mass translational movements will cause intensity fluctuations at the detector. However, as $X_r \to 1$, the characteristic molecular size becomes comparable to $1/K$, allow-

Table III
Molecular Parameters in Dilute Solution (I)

sample	$M_{w,app} \times 10^{-6}$	$M_w \times 10^{-6}$	$10^4 A_{2,app}$, mol cm^3 g^{-2}	$10^4 A_2$, mol cm^3 g^{-2}	R_g, nm	A_p, cm^3/g	$10^3 C^*$, g/cm^3
S1	9.00	11.25[a]	3.3	2.7[b]	280		0.83
S2	6.60	8.25[a]	3.6	2.9[b]	200		1.72
S3	2.00		4.0	3.2[b]	95	−0.30	4.84
S3 (110°)		2.50		3.1	94		
S4	1.25		4.5	3.6[b]	80	−0.29	
S4 (170°)	1.31		4.2		80[c]	−0.31	
S4 (140°)	1.40		4.0[b]		79[c]	−0.30	
S4 (110°)		1.56		3.6	79		5.06
S5	0.75		4.6	3.8[b]	57	−0.27	
S5 (170°)	0.77		4.5[b]		57[c]	−0.29	
S5 (140°)	0.81		4.3[b]		57[c]	−0.30	
S5 (110°)		0.90		3.8	56		5.57

[a] Calculated by eq 27. [b] Calculated by eq 28. [c] Calculated by using the radius of gyration determined at finite concentration divided by $1 + 2A_2M_wC$.

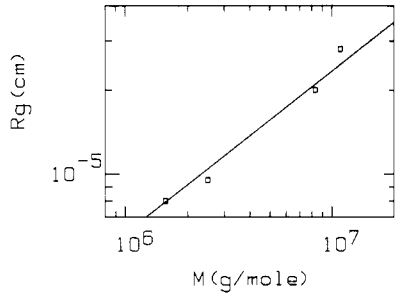

Figure 10. log–log plot of radius of gyration vs. molecular weight. Solid line is represented by R_g (cm) = $2.04 \times 10^{-9} M_w^{0.58}$.

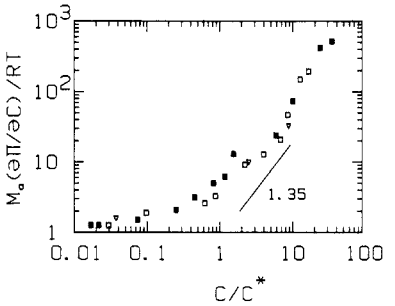

Figure 11. log–log plot of $M_a(\partial\pi/\partial C)/RT$ vs. C/C^* for sample S1 (open squares), sample S2 (filled squares), and sample S3 (inverted open triangles). $M_a = M_{app}$.

ing intramolecular motions to modulate the scattered intensity. Static light scattering measures the time average of this molecular self-interference through the term $P(X_r)$. For a Gaussian random coil

$$P(X_r) = (2/X_r^2)(\exp(-X_r) + X_r - 1) \qquad (29)$$

Figure 10 shows a log–log plot of radius of gyration vs. molecular weight. From this plot and with a four-point fit, we get a scaling relation, R_g (cm) = $1.18 \times 10^{-9} M_w^{0.62}$. however, α_R should be less than 0.60. Also the high molecular weight region deviated from linearity. With only the three data points, R_g (cm) = $3.02 \times 10^{-9} M_w^{0.55}$. From this analysis, we estimated $\alpha_R \sim 0.58 \pm 0.04$ and concluded the mixed solvent HCTP/TCB to be a relatively good solvent for PDP. Positive and relatively temperature-independent values of A_2 as listed in Table III also confirm this observation. More precise data can undoubtedly be achieved. However, our main aim is trying to establish a procedure that will permit us to study the solution polymerization of HCTP in TCB. Thus, the present estimate should suffice.

From the preferential adsorption data, TCB appears to have a better solvent quality than HCTP for the PDP polymer. The same can also be applied to examine the relationship between the second virial coefficient and the molecular weight. We found A_2 (mol cm^3 g^{-2}) = $2.56 \times 10^{-3} M_w^{-0.14}$. The A_2 values are reasonable in insofar as the mixed solvent is a better solvent for lower molecular weight PDP.

The linear concentration behavior suggesting a constant value for the second virial coefficient at each molecular weight in the two Zimm plots, as shown in Figures 7 and 9, supports our supposition that the molecular weight of the polymer indeed remains relatively constant. In semidilute solutions, we would like to examine the static property of the polymer solution in terms of $M(\partial\pi/\partial C)/RT$ as a function of reduced concentration C/C^*, where C^* ($\sim M/N_A R_g^3$) is the overlap concentration as shown in Figure 11 and Table III. The universal curve[19-28] in the molecular weight range that we have illustrated can be represented by straight lines over limited C/C^* ranges in the semidilute solution regime, as shown in Figure 11. Measurements of the osmotic compressibility in semidilute solutions permit us to determine the polymer concentration independent of the polymer molecular weight. The solid straight line in Figure 11 can be represented by $M(\partial\pi/\partial C)/RT = k_M(C/C^*)^m$, where m has an initial slope of 1.35 near $C/C^* \sim 1$. According to the scaling relation, $m = 1/(3\alpha_R - 1) = 1.35$ for $\alpha_R = 0.58$ and $R_g = k_R M^{\alpha_R}$. The crossover region is very broad from dilute to semidilute concentrations. We note that in the limit of zero concentration

$$\lim_{C \to 0} \frac{1}{RT}\left(\frac{\partial \pi}{\partial C}\right) = \frac{1}{M_{w,app}} \qquad (30)$$

Therefore, the universal curve in Figure 11 starts at values that are slightly higher than 1 in dilute concentrations and increases with increasing concentration because of a positive $A_{2,app}$ in good solvent, such as our system of PDP in HTCP/TCB. However, $A_{2,app}$ is related to M and C^*. So, the universal curve is valid over the entire concentration range from dilute to semidilute solutions, including the crossover region. More quantitative theory using renormalization group techniques have been reported.[19-21]

With renormalization group techniques, the universal curve in the good solvent limit can be described by a continuous curve and has the form

$$\frac{M_w}{RT}\frac{\partial \pi}{\partial C} = 1 + \frac{1}{8}\left\{9X - 2 + \frac{2\ln(1+X)}{X} \times \exp\left\{\frac{1}{4}\left[\frac{1}{X} + 1 - \frac{1}{X^2}\ln(1+X)\right]\right\}\right\} \qquad (31)$$

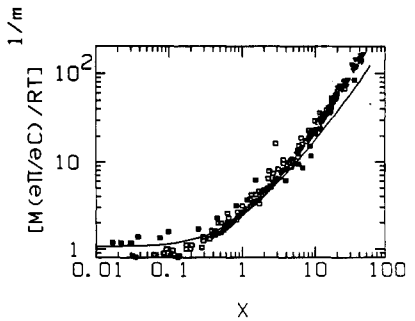

Figure 12. log–log plot of $[M(\partial\pi/\partial C)/RT]^{1/m}$ vs. X for PST/MEK and PST/toluene (open squares), PDP/HCTP/TCB (filled squares), and PMMA/MMA (inverted open triangles). Solid line was calculated according to eq 31. Note: PST/MEK and PST/toluene data were taken from ref 20 and scaled by $m = 1.12$. PMMA/MMA data were taken from ref 13 and scaled by $m = 1.61$. PDP/HCTP/TCB data were scaled by $m = 1.41$. Theoretical curve was scaled by $m = 1.10$.

where $X = Q(C/C^*)$, with Q being a constant. Q can be estimated according to

$$X[\tfrac{9}{16} - \tfrac{1}{8} \ln (M_w/M_n)] = A_2 M_w C \qquad (32)$$

Figure 12 shows a comparison between the theory and our PDP in HCTP/TCB and literature data on PMMA/MMA, polystyrene (PST)/toluene, and PST/MEK. In order to make a comparison among different solvent qualities, we arbitrarily scaled the y axis to a power of $1/m$, and for the HCTP/TCB system we used $M_{w,app}$ insterad of M_w in order to achieve the same effective quantity: $1 + 2A_2M_wC = 1 + 2A_{2,app}M_{w,app}C$ in the dilute solution region. It should also be noted that from the calculations we should have $Q = 4$ and 16 for PDP/HCTP/TCB and PMMA/MMA, respectively. However, we used $Q = 1$ and 6 for PDP/HCTP/TCB and PMMA/MMA in order to get a better fit. As discussed in ref 13 for polymer viscoelastic fluids, the crossover concentration C_e (an entanglement concentration in shear viscosity) represents a better indication for the onset of entanglement behavior. In Θ solutions, $C_e < C^*$. It is suggested that in the calculation for Q we should use C_e instead of C^*, which will give us a lower Q value, consistent with what we have used in computing m. In fairly good solvents, Figure 12 can be used to extract the polymer concentration from measurements of absolute scattered intensity at zero scattering angle ($R_{vu}(\theta \to 0)$) provided that the refractive index increment of the polymer/solvent system is known. While theory deals mainly with monodisperse polymers, experiments on both the solution polymerization of HCTP/TCB yielding PDP and on the thermal polymerization of MMA yielding PMMA revealed fairly broad molecular weight distributions; i.e., $M_w/M_n \sim 2$. In constructing this particular universal curve, we have implicitly assumed that the polydispersity effect is negligible since the osmotic pressure is independent of molecular weight in semidilute solutions. The fact that the data points do overlap suggest that it is valid for us to make such a supposition. Furthermore, the agreement between the theoretical and the experimental values for m at $C/C^* \sim 1$ strengthens our supposition (i.e., relatively constant molecular weight during the polymerization process), which will again be verified by our light scattering line width measurements. It should be noted that once we have demonstrated such a universal curve from experiments, its utility is not restricted to any particular polymer. The application can certainly be extended to polymer products with fairly constant broad molecular weight distributions.[29] Changes of polydispersity will invariably affect the crossover region in the universal curve. Furthermore, the universal curve is likely to break down if we try to approach the Θ condition or to go below the Θ temperature for high molecular weight polymers, where we may encounter critical effects in the crossover region.[13]

Spectrum of Scattered Light. In the initial analysis, we used the second-order cumulants method[30] with

$$Ab|g^{(1)}(\tau)|^2 = Ab \exp\{2[-\bar{\Gamma}\tau + (1/2)(\mu_2/\bar{\Gamma}^2)(\bar{\Gamma}\tau)^2]\} \qquad (33)$$

where $\bar{\Gamma} = \int \Gamma G(\Gamma)\, d\Gamma$ and $\mu_2 = \int G(\Gamma)(\Gamma - \bar{\Gamma})^2\, d\Gamma$. In semidilute solutions, we have used single exponentials to determine the characteristic line width Γ from $g^{(1)}(\tau)$. The $\bar{\Gamma}$ and $\mu_2/\bar{\Gamma}^2$ values are and should be in reasonable agreement using the method of cumulants and the regularization model because both approaches try to take into account the polydispersity effect. The cumulants method can provide information such as the average line width ($\bar{\Gamma}$) and the variance ($\mu_2/\bar{\Gamma}^2$), which is related to the width of the characteristic line width distribution. The method of regularization[6] will give us the distribution function without an apriori assumption on the form of $G(\Gamma)$ and is particularly suitable for analysis of unimodal distributions of reasonable variance; e.g., $\mu_2/\bar{\Gamma}^2 \sim 0.1$–1.

In semidilute solutions, the faster cooperative diffusion coefficient D_c is independent of molecular weight and can, in essence, be fitted with a single-exponential function. Figure 13 shows typical correlation functions and percent deviation for sample S3 at concentration $C = 2.24 \times 10^{-3}$, 0.014, and 0.021 g/cm^3, respectively. The relative deviation was defined by

$$\%\ \text{dev} = \frac{(Ab)^{1/2}|g^{(1)}(\tau)|_{\text{measd}} - (Ab)^{1/2}|g^{(1)}(\tau)|_{\text{calcd}}}{(Ab)^{1/2}|g^{(1)}(\tau)|_{\text{measd}}} \qquad (34)$$

In obtaining the normalized first-order correlation function, we used $G^{(2)}(\tau) = A(1 + b|g^{(1)}(\tau)|^2)$, where A is a background and the quantity b is treated as an adjustable parameter. For a polymer solution at finite concentrations this parameter not only depends on optical geometry but also on concentration effects. More specifically it depends on the relative intensity ratio of the polymer solution to that of the pure solvent. Following the argument by Tanaka,[31] this concentration effect can be expressed by

$$G^2(\tau) = (a_2 + a_3)^2 + b[a_2 \exp(-\tau\Gamma_2) + a_3 \exp(-\tau\Gamma_3)]^2 \qquad (35)$$

where a_2 is the scattering intensity of the solvent, a_3 is that of the solute, Γ_2 and Γ_3 are the respective characteristic line width ($\Gamma_i = D_iK^2$, with D_i being the diffusion coefficient of i), and b is an efficiency factor determined by the scattering geometry. In high polymer solutions, the solvent molecules are much smaller than the solute molecules and have a much larger diffusion coefficient. Thus, the autocorrelation function due to the solvent molecules has a much shorter relaxation time. With $\Gamma_3 \ll \Gamma_2$ in eq 35, the measurable correlation function is reduced to

$$G^2(\tau) \cong (a_2 + a_3)^2\{1 + b[a_3/(a_2 + a_3)]^2(\exp(-\tau\Gamma_3))^2\} \qquad (36)$$

Thus, at finite concentrations the original factor b should be modified by a factor of $(1 + a_2/a_3)^2$. In order to get the correct instrument constant (b), one should use a polymer solution with $a_3 \gg a_2$, such as an aqueous suspension of polystyrene latex spheres.

In a log–log plot of $b|g^{(1)}(\tau)|^2$ vs. K^2 or in a plot $\bar{\Gamma}$ vs. K^2, we see that the K^2 dependence holds for sample S4 as shown in Figure 14. This procedure allows us to extrapolate the diffusion coefficient to zero scattering angle. The concentration dependence of the diffusion coefficient in

Table IV
Molecular Parameters in Dilute Solution (II)

sample	$M_w \times 10^{-6}$	$D_0 \times 10^7$, cm^2/s	R_g, nm	R_h, nm	R_h/R_g	k_d, mL/g	C_D	M_w/M_n
S1								1.74
S2	8.25	0.48	200	128	0.64	9.9×10^2	5.95	1.66
S3	2.50	0.97	95	63	0.67	-50	6.47	1.59
S4	1.56	1.26	80	49	0.61	-43	6.27	1.27
S5	0.90	1.77	57			-35		1.15

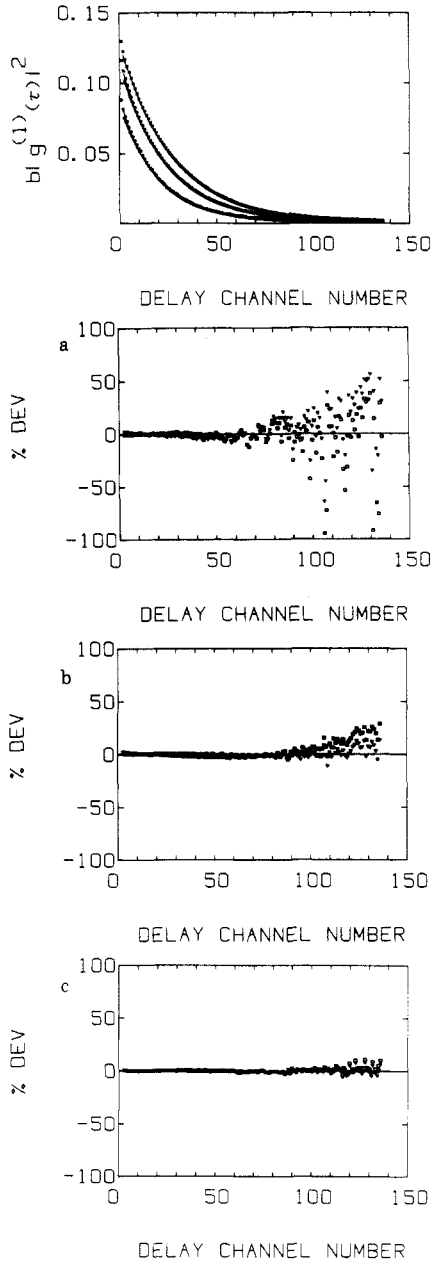

Figure 13. Typical plots of $b|g^{(1)}(\tau)|^2$ and percent deviation vs. delay channel number for sample S3. The numerical results described in a, b, and c correspond to the bottom, middle, and top curves, respectively. (a) Delay time increment, $\Delta\tau = 40$ μs (the solid curve is represented by $b|g^{(1)}(\tau)|^2 = 2.99 \times 10^{-1}$ exp2[$-3.43 \times 10^2\tau + {}^1/_2(2.88 \times 10^4)\tau^2$], with τ expressed in μs, and the dash double dot curve is represented by $b|g^{(1)}(\tau)|^2 = 2.88 \times 10^{-1}$ exp2[$-(5.95 \times 10^2)]\tau$). (b) $\Delta\tau = 40$ μs (the solid curve is represented by $b|g^{(1)}(\tau)|^2 = 3.42 \times 10^{-1}$ exp2[$-2.78 \times 10^2\tau + {}^1/_2(1.63 \times 10^4)\tau^2$] and the dash double dot curve is represented by $b|g^{(1)}(\tau)|^2 = 3.33 \times 10^{-1}$ exp2[$-(5.00 \times 10^2)]\tau$). (c) $\Delta\tau = 40$ μs (the solid curve is represented by $b|g^{(1)}(\tau)|^2 = 3.60 \times 10^{-1}$ exp2[$-2.37 \times 10^2\tau + {}^1/_2(3.58 \times 10^3)\tau^2$] and the dash double dot curve is represented by $b|g^{(1)}(\tau)|^2 = 3.60 \times 10^{-1}$ exp2[$-(4.60 \times 10^2)]\tau$). In the deviation plots, parts a, b, and c have open squares representing single-exponential fits. All inverted open triangles represent second-order cumulants fit.

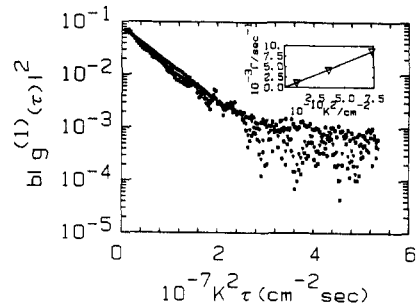

Figure 14. Correlation function $b|g^{(1)}(\tau)|^2$ at $\theta = 30°$ (filled squares), $\theta = 60°$ (inverted filled triangles), and $\theta = 90°$ vs. delay time as scaled by K^2. For sample S4 at concentration $C = 1.23 \times 10^{-3}$ g/cm^3, the inset shows the K^2 dependence of $\bar{\Gamma}$.

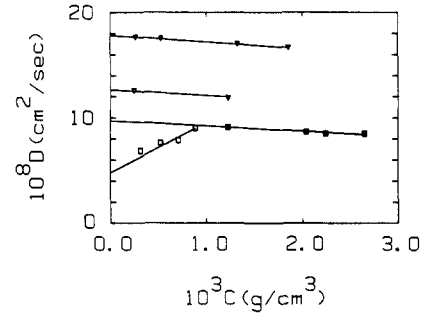

Figure 15. Extrapolation of D to zero concentration for sample S2 (open squares), S3 (filled squares), S4 (inverted open squares), S5 (inverted filled squares). The corresponding values of D_0 and k_d are listed in Table IV.

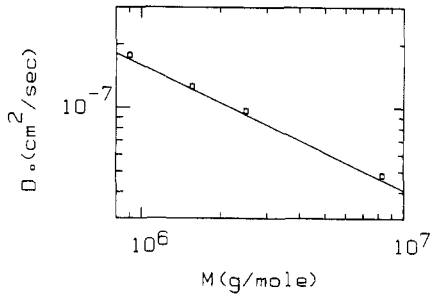

Figure 16. log–log plot of diffusion coefficient vs. molecular weight. The solid line is represented by D_0 (cm^2/s) = $5.49 \times 10^{-4} M_w^{-0.58}$.

dilute solution can be expressed adequately with a first-order expansion in concentration as described by eq 10 and is illustrated in Figure 15. The corresponding hydrodynamic radius R_h can then be computed with the Stokes–Einstein relation as described in eq 7 and 8.

Results from dynamic measurements are summarized in Table IV. The scaling relation for PDP in HCTP/TCB was determined to be D_0 (cm^2/s) = $5.49 \times 10^{-4} M_w^{0.58}$ as shown in a log–log plot of D_0 vs. molecular weight (Figure 16) or R_h (cm) = $1.25 \times 10^{-9} M_w^{0.58}$. The agreement between the empirical relations (α_D and α_R) as determined by dynamic and static light scattering measurements shows the self-consistency of our experimental results. In our analysis, we have assumed PDP to be essentially linear or

the degree of branching to be constant, if its exists. This assumption is valid especially when the fractional conversion of monomer to polymer (f_p) is less than 50%. In our case, $f_p < 25\%$. The α_D result confirms that our estimate on α_R without full weighing of the fourth high molecular weight value is reasonable. The coil expansion factor R_h/R_g can be checked by comparing our experiments with the current therory,[32] which predicts that R_h/R_g is closely related to the scaling relation

$$\frac{R_h}{R_g} = \frac{\pi^{1/2}}{2(3^{1/2})}(2 - \alpha_D)(1 - \alpha_D)[(\alpha_D + 1)(2\alpha_D + 1)]^{1/2} \quad (37)$$

From the static and dynamic light scattering measurements described above, α_D has an estimated value of $\sim 0.58 \pm 0.4$. As a result R_h/R_g should have a value close to 0.56, which is lower than the experimental value listed in Table IV. This discrepancy in a mixed solvent might be due to the preferential adsorption effect. The preferential adsorption coefficient determined from static measurements is about 0.3 for PDP in HCTP/TCB. This value represents the ratio of the volume occupied by the excess molecules of the good solvent surrounding a polymer to the mass of the polymer molecule. It is known that, within a volume V_h ($=4\pi R_h^3/3$) surrounding a polymer molecule, the fraction occupied by the excess solvent molecules is $A_p M_w/V_h N_A$. Therefore in the range of our study, this fraction has a value of $61 M_w^{-0.74}$. It means that only about 0.3% of the volume is preferentially adsorbed by the polymer. Thus, the fact that the ratio R_h/R_g is about 5%–13% greater than the theoretically predicted value is probably not due to preferential adsorption. It is interesting to note that such a discrepancy has also been reported in the literature[33–35] in a series of studies of polystyrene in a mixed Θ solvent.

The second virial coefficient for diffusion (k_d) as listed in Table IV shows a strong molecular weight dependence and changes from positive to negative. In order to check this trend a semiempirical expression for k_d was used

$$k_d = 2A_2 M_w - C_D N_A V_h / M_w \quad (38)$$

where C_D is a semiempirical constant that we are able to determine experimentally. Many theories have been presented to evaluate C_D. For example, $C_D = 1.0$[36,37] or 2.36[39] for coils and 7.16[38] and 6.99[39–41] for hard spheres. The C_D obtained by us has a value of about 6, which is higher than the theoretical value for coils. However, this nearly constant C_D value suggests that the trend for k_d from positive to negative is reasonable. It may be interesting to note that independent work has been done in our laboratory showing a C_D value of 6.61 for poly(ethylene terephthalate) (PET) in a good solvent hexafluoro-2-propanol (HFIP).[42] The discrepancy between these experimental values and theory is an open question.

The dynamic measurements for PDP/HCTP/TCB is also performed at different temperatures below 215 °C when we quenched the polymerization reaction. A typical plot of the first-order correlation function at the same concentration but different temperatures for sample S4 is shown in Figure 17. From the static data as listed in Table III we found that the second viral coefficient and the radius of gyration is relatively independent of temperature. Therefore, it is reasonable to assume that the temperature dependence of k_d and R_h is also quite small. Then, the viscosity of the mixed solvent at high temperatures can be calculated with the Stokes–Einstein relation. The calculated values of viscosity were then plotted on top of the viscosity–temperature plot for the mixed solvent as shown in Figure 3. We can see that the calculated values

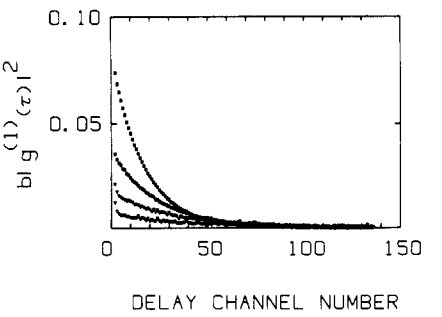

Figure 17. Correlation function $b|g^{(1)}(\tau)|^2$ at 215 °C (open squares), 170 °C (filled squares), 140 °C (inverted open triangles), and 110 °C (inverted filled triangles) for sample S4 at concentration $C = 1.96 \times 10^{-3}$ g/cm^3, scattering angle $\theta = 30°$, and delay time increment $\Delta\tau = 40$ μs.

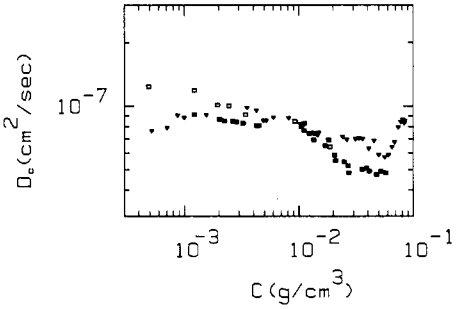

Figure 18. log–log plots of cooperative diffusion coefficient D_c vs. concentration for sample S2 measured at $\theta = 45°$ (inverted filled triangles), S3 measured at $\theta = 30°$ (filled squares), and S4 measured at $\theta = 30°$ (open squares). $\Gamma = DK^2$.

agree well with the extrapolated curve. The small deviation may be due to the change in solvent composition and the small temperature dependence of k_d and R_h. However, the agreement again confirms the self-consistency of our results and analysis.

The cooperative diffusion coefficient of PDP in HCTP/TCB in semidilute solutions is a decreasing function of concentration as shown in Figure 18. This behavior is quite different from our previous study[13] of thermal polymerization of poly(methyl methacrylate)/methyl methacrylate but is similar to the thermal polymerization of poly(styrene)/styrene system.[43] The decrease in cooperative diffusion cannot be explained by scaling law. However, as described in ref 12, the interpretation and measurements of the cooperative diffusion coefficient may be more complex[44] because of the transient network lifetime τ_R. There are two distinct elastic moduli in polymer solutions at semidilute concentrations

$$D_c = [K_{os} + (4/3)G]/f \quad (39)$$

where K_{os}, G, and f are respectively the osmotic modulus, the shear modulus, and the friction coefficient with concentration dependences of $K_{os} \sim C^3$, $G \sim C^2$, and $f \sim C^2$ in the Θ region. In order to understand the PDP behavior in the semidilute region more detailed experiments should be performed.

Molecular Weight Distribution Analysis. In dilute solution, the characteristic line width distribution function can be related to the molecular weight distribution function.[5,6] Thus it is worthwhile to make an approximate Laplace inversion of $g^{(1)}(\tau)$ using the regularization method. A typical plot of the first-order correlation function according to such a fitting procedure as well as the deviation between computed and experimental values is shown in Figure 19. By taking into account intraparticle interference and concentration effects, we get a plot of $G(D_0)$ vs. D_0 as shown in Figure 20, which can be transformed

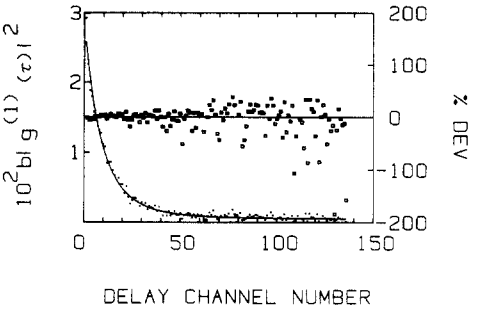

Figure 19. Plot of $b|g^{(1)}(\tau)|^2$ and percent deviation vs. delay channel number for the sample S4 at concentration $C = 2.22 \times 10^{-4}$ g/cm^3 and scattering angle 30°. Numerical values ($G(\Gamma)$) from the regularization fit are presented in Figure 20. In the percent deviation plot, data are denoted by open squares.

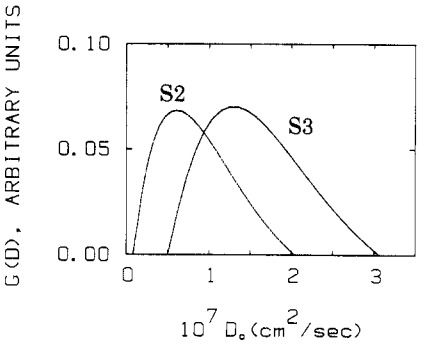

Figure 20. Unnormalized line width distribution for sample S2 at $C = 1.27 \times 10^{-4}$ g/cm^3 and $\theta = 45°$ and S3 at $C = 2.22 \times 10^{-4}$ g/cm^3 and $\theta = 30°$. Note that we have used eq 10 to shift the x axis to D_0 [$=D/(1 + k_dC)$] with $k_d = 9.9 \times 10^2$ cm^3/g for S2 and $k_d = -44$ cm^3/g for S4, respectively.

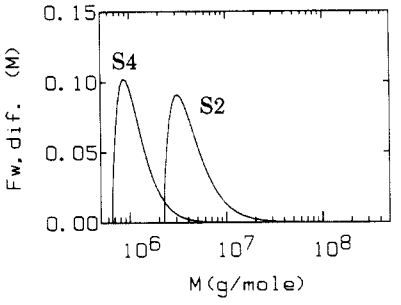

Figure 21. Molecular weight distributions for sample S2 and S4 with $\alpha_D = 0.57$ based on the analysis of Figure 20.

Table V
Effects of α_D on the Polydispersity Index M_w/M_n for Sample S4

α_D	M_w/M_n	α_D	M_w/M_n
0.50	1.31	0.57	1.27
0.52	1.30	0.58	1.26
0.54	1.29	0.60	1.25
0.56	1.28		

into a plot of $F_{w,dif}$ vs. M, where $F_{w,dif}$ is the polymer differential molecular weight distribution with $\alpha_D = 0.58$. Figure 21 shows the molecular weight distributions of PDP obtained by solution polymerization in HCTP/TCB on two different runs (samples S2 and S4 with $\alpha_D = 0.57$). The consistency of our results can best be expressed in Table V, which shows the effect of α_D on the polydispersity index M_w/M_n and in Figure 22, showing its effect on the molecular weight distribution. For $\alpha_D \sim 0.58$, $M_w/M_n \sim 1.26$ for sample S3 and is in very good agreement with the GPC results.[11] Figure 23 shows the cumulative molecular weight distribution $F_{w,cum}$ based on the results of

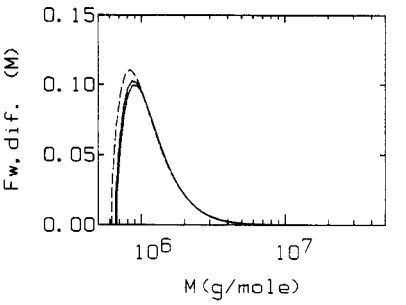

Figure 22. Molecular weight distributions for sample S4 with $\alpha_D = 0.5$ (dashed curve), $\alpha_D = 0.57$ (solid curve), and $\alpha_D = 0.6$ (dash double dot curve).

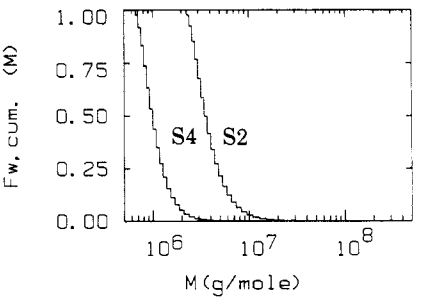

Figure 23. Cumulative molecular weight distributions for sample S2 and S4 based on the analysis of Figure 21.

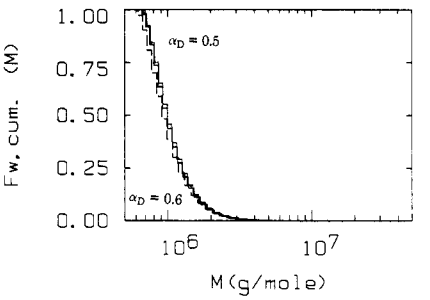

Figure 24. Cumulative molecular weight distributions for sample S4 with $\alpha_D = 0.5$, $\alpha_D = 0.57$ (solid histogram), and $\alpha_D = 0.6$ based on the analysis of Figure 22.

Figure 21. The molecular weight of PDP varies over a factor of about 30 for the different runs. It should be recognized that the value of M_w/M_n increases with decreasing α_D values as listed in Table V and shown schematically in Figures 22 and 24. However, with small variations in α_D, such as 0.57–0.59, the results of our studies remain essentially the same and certainly within our error limits.

Conclusions

We have investigated many of the macromolecular parameters of PDP in HCTP/TCB during the solution polymerization of HCTP using a combination of Raman spectroscopy and laser light scattering. Our results are internally consistent in terms of exponent relationships for different molecular parameters. For solution polymerization, we have been able to determine the molecular weight distribution of PDP as well as $M_{w,app}$, $A_{2,app}$, R_g, and k_d in dilute solutions, provided that the PDP molecular weight has remained relatively constant during the polymerization process. The trends in concentration dependence of the osmotic compressibility $(\partial\pi/\partial C)_{T,P}$ and of the translational diffusion coefficient D seem to strengthen this supposition. By quenching the reaction and by matching the refractive index of the two solvent components in the solvent mixture, we were able to determine M_w and A_2 and to calculate the amount of pref-

erential adsorption. In semidilute solutions, the accessible quantities, such as the osmotic compressibility $(\partial\pi/\partial C)_{T,P}$ and the cooperative diffusion coefficient D_c, become independent of polymer molecular weight. However, these quantities, while no longer properties of polymer molecular weight, can be used to compute polymer concentration if a correspondence relationship is known. Thus, we have demonstrated a scheme whereby we can indeed investigate pertinent macromolecular parameters during solution polymerization. This scheme can be extended to all the solution polymerization processes (additional type mechanism), as long as one can find an isorefractive point for the mixed solvent or calibrate the molecular weight by other means.

So far, we have demonstrated two general schemes to handle thermal polymerization[13] and solution polymerization (this work). In both cases we examined the additional type of polymerization, in which the molecular weight remains relatively a constant during the reaction (in the absence of a gel effect). Such schemes can be extended to other classes of polymerization (living, combination) in which the molecular weight becomes a function of time. For example, eq 1 can be modified as

$$\lim_{K\to 0} \frac{HC}{R_{vu}} = \frac{1}{M_w} + 2k_A M_w^{-\alpha_A} C \qquad (40)$$

if $A_2 = k_A M_w^{-\alpha_A}$ can be determined in advance. The constants k_A and α_A are system specific.

In dynamic measurements, eq 10 can be modified as

$$D = D_1 M_w^{-\alpha_D} + D_2 M_w^{-\alpha_D-\alpha_A+1} + D_3 M_w^{-\alpha_D-3\alpha_h-1} \qquad (41)$$

with

$$D_1 = k_D$$

$$D_2 = 2k_A k_D C$$

$$D_3 = -\frac{4\pi}{3} C_D N_A k_h^3 C k_D$$

and k_h and α_h being the coefficients for the scaling relation $R_h = k_h M_w^{\alpha_h}$. As eq 40 and 41 are functions of M_w alone, we should be able to follow the molecular weight change during the reaction in the dilute solution regime. Our combined scattering techniques allow us to measure the kinetic effect (Raman), the thermodynamic effect (intensity), and the hydrodynamic effect (line width). The potential of such a combination (Raman/intensity/line width) to study the polymerization processes has now been demonstrated by the present study using PDP in HCTP/TCB at 215 °C.

Acknowledgment. We gratefully acknowledge the US Army Research Office for support of this research project and Professor G. Fytas, who assisted during the initial phase of this experiment.

Registry No. HCTP, 940-71-6; PDP (SRU), 26085-02-9; HCTP (homopolymer), 25231-98-5; TCB, 120-82-1.

References and Notes

(1) Huglin, M. B., Ed. *Light Scattering from Polymer Solutions*; Academic: New York, 1972.
(2) Chu, B. In *Scattering Techniques Applied to Supramolecular and Nonequilibrium Systems*; Chen, S.-H., Chu, B., Nossal, R., Eds.; Plenum: New York, 1981; pp 231–264.
(3) Chu, B. In *Proceedings of the NATO Advanced Study Institute on the Application of Laser Light Scattering to the Study of Biological Motions*; Earnshaw, J. C., Steer, M. W., Eds.; Plenum: New York, 1983; pp 53–76.
(4) Ford, J. R.; Chu, B. In *Proceedings of the 5th International Conference on Photon Correlation Techniques in Fluid Mechanics*; Schulz-DuBois, E. O., Ed.; Springer-Verlag: New York, 1983; pp 303–314.
(5) Chu, B.; Ford, J. R.; Pope, J. *Annu. Tech. Conf. Soc. Plast. Eng.* **1983**, *26*, 547.
(6) Chu, B.; Ford, J. R.; Dhadwal, H. S. *Methods Enzymol.*, in press.
(7) Allcock, H. R.; Best, R. J. *Can. J. Chem.* **1962**, *42*, 447.
(8) Lund, L. G.; Paddock, N. L.; Proctor, J. E.; Searle, H. T. *J. Chem. Soc.* **1960**, 2542.
(9) Griffing, V.; Cargyle, M.; Corvese, L.; Eby, D. *J. Phys. Chem.* **1954**, *58*, 1054.
(10) Allcock, H. R.; Arcus, R. A. *Macromolecules* **1979**, *12*, 1130.
(11) Hagnauer, G. L.; Koulouris, T. N. *Chromatogr. Sci.* **1981**, *19*, 99.
(12) Chu, B.; Fytas, G. *Macromolecules* **1982**, *15*, 561.
(13) Chu, B.; Lee, D.-C. *Macromolecules* **1984**, *17*, 926.
(14) Tuzar, Z.; Kratochvil, P. *Collect. Czech. Chem. Commun.* **1967**, *32*, 3358.
(15) Kratochvil, P.; Strakova, D.; Stegskal, J.; Tuzar, Z. *Macromolecules* **1983**, *16*, 1136.
(16) Outer, P.; Carr, C. I.; Zimm, B. H. *J. Chem. Phys.* **1950**, *18*, 830.
(17) Strazielle, C.; Benoit, H. *J. Chem. Phys.* **1961**, *58*, 678.
(18) Cowie, J. M. G.; Bywater, S. *J. Macromol. Chem.* **1966**, *1*, 581.
(19) Oono, Y.; Ohta, T.; Freed, K. F. *J. Chem. Phys.* **1981**, *74*, 6488.
(20) Wiltzius, P.; Haller, H. R.; Cannell, S. D. *Phys. Rev. Lett.* **1983**, *51*, 1183.
(21) Ohta, T.; Oono, Y. *Phys. Lett.* **1982**, *89A*, 460.
(22) des Cloizeaux, J.; Noda, I. *Macromolecules* **1982**, *15*, 1505.
(23) Noda, I.; Kato, N.; Kitano, Y.; Nagasawa, M. *Macromolecules* **1981**, *14*, 668.
(24) Noda, I.; Higo, Y.; Ueno, N.; Fujimoto, T. *Macromolecules* **1984**, *17*, 1055.
(25) Schafer, I. *Macromolecules* **1982**, *15*, 652.
(26) Schafer, I. *Macromolecules* **1984**, *17*, 1357.
(27) Stepanek, P.; Perzynski, R.; Delsanti, M.; Adam, M. *Macromolecules* **1984**, *17*, 2340.
(28) Amirzadek, J.; McDonnell, M. E. *Macromolecules* **1982**, *15*, 927.
(29) Chu, B.; Nose, T. *Macromolecules* **1980**, *13*, 122.
(30) Koppel, D. E. *J. Chem. Phys.* **1972**, *57*, 4814.
(31) Sun, S.-T.; Nishio, I.; Swislow, G.; Tanaka, T. *J. Chem. Phys.* **1980**, *73*, 5971.
(32) Benmouna, M.; Akcasu, A. Z. *Macromolecules* **1978**, *11*, 1187.
(33) Lacharojana, S.; Caroline, D. *Macromolecules* **1977**, *10*, 365.
(34) Jones, G.; Caroline, D. *Chem. Phys.* **1979**, *40*, 153.
(35) Jones, G.; Caroline, D. *Chem. Phys.* **1979**, *37*, 187.
(36) Yamakawa, J. *J. Chem. Phys.* **1962**, *36*, 2995.
(37) Imai, S. *J. Chem. Phys.* **1969**, *50*, 2116.
(38) Pyun, C. W.; Fixam, M. *J. Chem. Phys.* **1964**, *41*, 937.
(39) Batchelor, G. K. *J. Fluid Mech.* **1972**, *52*, 245.
(40) Batchelor, G. K. *J. Fluid Mech.* **1976**, *74*, 1.
(41) Felderhof, B. U. *J. Phys. A., Math. Gen.* **1978**, *11*, 929.
(42) Naoki, M.; Park, I. H.; Wunder, S. L.; Chu, B. *J. Polym. Sci., Polym. Phys. Ed.*, in press.
(43) Patterson, G. D.; Stevens, J. R.; Alms, G. R.; Lindsey, C. P. *Macromolecules* **1979**, *12*, 658.
(44) Brochard, F. *J. Phys. (Les Ulis, Fr.)* **1983**, *44*, 39.